Acta Crystallographica Section F
Structural Biology and Crystallization Communications
ISSN 1744-3091

New structural insights and molecular-modelling studies of 4-methyl-5-β-hydroxyethylthiazole kinase from *Pyrococcus horikoshii* OT3 (*Ph*ThiK)

Jeyaraman Jeyakanthan,[a]* Subbiah Thamotharan,[b] Devadasan Velmurugan,[c] Vaijayanthimala Surya Narayna Rao,[c] Shanthi Nagarajan,[d] Akeo Shinkai,[e] Seiki Kuramitsu[e,f] and Shigeyuki Yokoyama[g,h]

[a]National Synchrotron Radiation Research Center, 101 Hsin-Ann Road, Hsinchu Science Park, Hsinchu 30076, Taiwan, [b]Molecular Biophysics Unit, Indian Institute of Science, Bangalore 560 012, India, [c]Centre of Advanced Study in Crystallography and Biophysics, University of Madras, Guindy Campus, Guindy, Chennai 600 025, India, [d]Bioinformatics Centre, Pondicherry University, Pondicherry 605 014, India, [e]RIKEN SPring-8 Center, Harima Institute, 1-1-1 Kouto, Sayo, Hyogo 679-5148, Japan, [f]Graduate School of Science, Osaka University, Toyonaka, Osaka 560-0043, Japan, [g]RIKEN Systems and Structural Biology Center, Yokohama Institute, 1-7-22 Suehiro-cho, Tsurumi, Yokohama 230-0045, Japan, and [h]Graduate School of Science, The University of Tokyo, 7-3-1 Hongo, Bunkyo-ku, Tokyo 113-0033, Japan

Correspondence e-mail: kanthan@spring8.or.jp

Received 3 September 2009
Accepted 7 September 2009

PDB Reference: 4-methyl-5-β-hydroxyethylthiazole kinase, 3hpd, r3hpdsf.

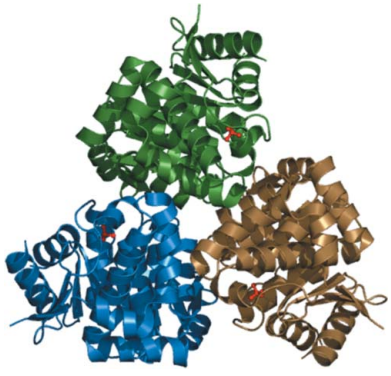

4-Methyl-5-β-hydroxyethylthiazole kinase (ThiK) catalyses the phosphorylation of the hydroxyl group of 4-methyl-5-β-hydroxyethylthiazole. This work reports the first crystal structure of an archaeal ThiK: that from *Pyrococcus horikoshii* OT3 (*Ph*ThiK) at 1.85 Å resolution with a phosphate ion occupying the position of the β-phosphate of the nucleotide. The topology of this enzyme shows the typical ribokinase fold of an α/β protein. The overall structure of *Ph*ThiK is similar to those of *Bacillus subtilis* ThiK (*Bs*ThiK) and *Enterococcus faecalis* V583 ThiK (*Ef*ThiK). Sequence analysis of ThiK enzymes from various sources indicated that three-quarters of the residues involved in interfacial regions are conserved. It also revealed that the amino-acid residues in the nucleotide-binding, magnesium ion-binding and substrate-binding sites are conserved. Binding of the nucleotide and substrate to the ThiK enzyme do not influence the quaternary association (trimer) as revealed by the crystal structure of *Ph*ThiK.

1. Introduction

Kinases are a ubiquitous group of enzymes that facilitate phosphoryl-transfer reactions from an ATP phosphate donor to an acceptor substrate. Thiamine is synthesized by most prokaryotes and by eukaryotes. In all cases, thiamine biosynthesis involves the separate formation of the pyrimidine and the thiazole. These are then coupled to form thiamine phosphate. A final phosphorylation catalyzed by 4-methyl-5-β-hydroxyethylthiazole kinase produces thiamine pyrophosphate (THI-PP), the biologically active form of the cofactor (Kawasaki, 1993). In bacteria, six gene products are involved in the formation of thiazole, whereas the formation of pyrimidine requires two. In contrast, only one gene product is required for biosynthesis of the thiazole and one for pyrimidine biosynthesis in yeast (Jurgenson *et al.*, 2009). Thiamine can be transported into the cell and can be salvaged through several routes.

Labelling studies in *Escherichi coli* and *Salmonella typhimurium* have demonstrated that the thiazole is formed from tyrosine (Estramareix & Therisod, 1972; Bellion *et al.*, 1976), deoxy-D-xylulose [without phosphate (David *et al.*, 1982; Himmeldirk *et al.*, 1996) or with phosphate (Nosaka *et al.*, 1994)] and cysteine (Tazuya, Yamada *et al.*, 1987). In *Bacillus subtilis*, the thiazole is formed from glycine rather than tyrosine (Tazuya, Morizaki *et al.*, 1987). The *de novo* biosynthesis of this small molecule is complex and involves at least six gene products (ThiFSGH, ThiI and Dxs), with an additional gene product (ThiM) involved in salvage of the thiazole from the medium (Begley *et al.*, 1999).

The 4-amino-5-hydroxymethyl-2-methylpyrimidine phosphate (HMP-P) ring is generated through a complicated rearrangement reaction catalyzed by ThiC using 5-aminoimidazole ribotide (AIR) as the substrate. ThiD then phosphorylates HMP-P to give HMP-PP. Thiamine monophosphate (ThMP) is formed through the coupling reaction of 4-methyl-5-β-hydroxyethylthiazole phosphate (THZ-P) and HMP-PP using ThiE. Thiamine phosphate kinase adds the final phosphate group to ThMP to give thiamine disphosphate (ThDP), the active form of the cofactor. This reaction is carried out by ThiL in an ATP-dependent manner (McCulloch *et al.*, 2008). ThDP can also be

formed from thiamine in one step using thiamine pyrophosphokinase. In bacteria, this enzyme is called ThiN. In higher organisms, the thiamine pyrophosphokinase is THI80. As an alternative to the *de novo* pathway, thiamine or the components of thiamine can be salvaged. In bacteria, the thiazole alcohol can be converted to THZ-P by thiazole kinase (ThiM). In addition, HMP can be converted to HMP-P by HMP-P kinase (ThiD). ThiD is also the enzyme that converts HMP-P to HMP-PP in the *de novo* pathway. In bacteria, thiamine can be converted to ThMP by thiamine kinase (ThiK) or to ThDP by thiamine pyrophosphokinase (ThiN; Jurgenson *et al.*, 2009).

Although sequence identity is not evident between ThiK enzymes from various sources (Fig. 1), they exhibit remarkable structural similarity and share a common nucleotide-binding and substrate-binding motif (Zhang *et al.*, 1997; Petersen & Downs, 1997). This enzyme is a member of the ribokinase family of sugar kinases and has a structure similar to those of pyridoxal kinase (Newman *et al.*, 2006), ribokinase (Sigrell *et al.*, 1998; Andersson & Mowbray, 2002) and adenosine kinase (Mathews *et al.*, 1998), as is evident from a *DALI* search (Holm & Sander, 1993). Thus, it is of interest to understand how phosphoryl transfer occurs in this particular group of enzymes and also to understand the variability and similarities between various ThiK enzymes.

The first detailed picture of the binding mode and catalytic reaction was obtained from the X-ray crystallograpic structure determination of complexes of the ThiK enzyme from *B. subtilis* (*Bs*ThiK) with the substrate THZ and ATP/THZ-P (Campobasso *et al.*, 2000). Recently, the coordinates of the structure of ThiK from the pathogenic bacterium *Enterococcus faecalis* V583 (*Ef*ThiK) complexed with ADP (PDB code 3dzv) have been deposited in the Protein Data Bank (http://www.rcsb.org) by the Joint Center for Structural Genomics (JCSG). Although several archaeal ThiK proteins have been identified, none of them have been structurally and/or functionally characterized. The present paper is the first crystal structure report of an archaeal ThiK protein: that from *Pyrococcus horikoshii* OT3 at 1.85 Å resolution.

2. Materials and methods

2.1. Expression and purification

The 4-methyl-5-β-hydroxyethylthiazole kinase (ThiK) protein from the archaeon *P. horikoshii* OT3 (*Ph*ThiK) used in this study has a molecular weight of 28.95 kDa and consists of 265 amino-acid residues. The plasmid encoding *Ph*ThiK was digested with *Nde*I and *Bgl*II and the fragment was inserted into the expression vector pET-11a (Novagen) linearized with *Nde*I and *Bam*HI. *Escherichia coli* BL21-CodonPlus(DE3)-RIL cells were transformed with the recombinant plasmid and grown at 310 K in Luria–Bertani medium containing 100 µg ml^{-1} ampicillin for 20 h. The transformants were cultured at 310 K overnight in a medium containing 1% polypeptone, 0.5% yeast extract, 0.5% NaCl, 100 µg ml^{-1} ampicillin pH 7.0 and 25 µg ml^{-1} chloramphenicol. The cells were lysed by sonication in 20 m*M* Tris–HCl pH 8.0 containing 500 m*M* NaCl, 5 m*M* β-mercaptoethanol and 1 m*M* phenylmethylsulfonyl fluoride (PMSF). The lysate was incubated at 363 K for 13 min and centrifuged at 15 000 rev min^{-1} for 30 min at 277 K.

After buffer-exchange by loading it onto a HiPrep 26/10 desalting column (GE Healthcare Biosciences) pre-equilibrated with 20 m*M* Tris–HCl pH 8.0, the protein sample was loaded onto a Toyopearl Super Q-650 M column (Tosoh) pre-equilibrated with 20 m*M* Tris–HCl pH 8.0. The protein bound to the column and was eluted with a linear gradient from 0 to 400 m*M* NaCl. The protein-containing fraction was subjected to buffer-exchange to 20 m*M* Tris–HCl pH 8.0 and was loaded onto a Resource Q column (GE Healthcare Biosciences) pre-equilibrated with the same buffer. The protein was bound to the column and eluted in a linear gradient from 0 to 400 m*M*

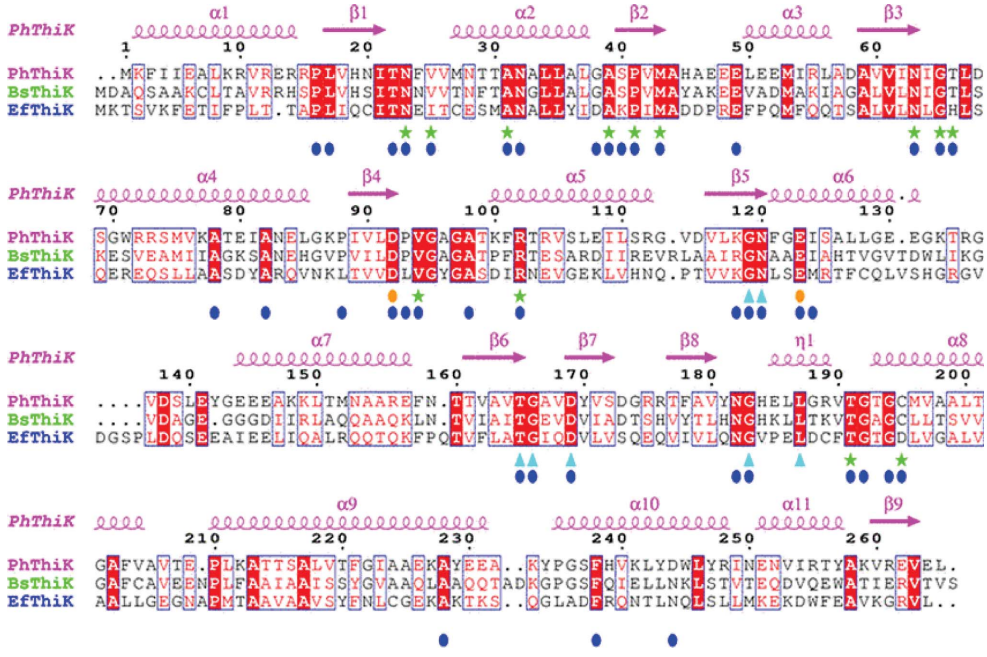

Figure 1
Sequence alignment of *Ph*ThiK with *Bs*ThiK (*B. subtilis* ThiK) and *Ef*ThiK (*En. faecalis* V583 ThiK) was performed using *ClustalW* (Thompson *et al.*, 1994) and the figure was produced using *ESPript* (Gouet *et al.*, 1999). The secondary-structural elements of *Ph*ThiK and residue numbering are shown above the sequence alignment. Sequence identities are highlighted in red and similarities are shown as red letters. Both identical and similar sequences are shown in blue boxes. The residues involved in the ATP, THZ-P and Mg^{2+} active sites of *Bs*ThiK, *Ph*ThiK and *Ef*ThiK are indicated by green stars, cyan triangles and orange circles, respectively. The conserved residues in 131 unique sequences of various ThiKs are indicated by blue circles.

Table 1
Data-collection and refinement statistics.

Values in parentheses are for the highest resolution shell.

Data statistics	
Space group	*I*23
Resolution (Å)	1.85
Unit-cell parameters (Å, °)	$a = b = c = 112.24$, $\alpha = \beta = \gamma = 90$
V_M (Å^3 Da^{-1})	2.1
Solvent content (%)	40.4
Resolution range (Å)	30.0–1.85 (1.92–1.85)
Measured reflections	81063
Unique reflections	20162 (2004)
R_{merge}† (%)	6.7 (29.2)
Completeness (%)	99.8 (99.5)
Average $I/\sigma(I)$	19.5 (4.4)
Redundancy	4.0 (3.9)
Refinement statistics	
Resolution (Å)	20.0–1.85
R_{work} (%)	16.4
R_{free} (%)	18.4
Protein atoms	1950
Water molecules	208
Phosphate ion	1
R.m.s.d. bond lengths (Å)	0.005
R.m.s.d. bond angles (°)	1.30
Estimated coordinate error (Å)	0.16
Overall *B* factor (Å^2)	18.90
Ramachandran plot (%)	
Most favoured	94.7
Allowed	5.3
PDB code	3hpd

† $R_{merge} = \sum_{hkl}\sum_i |I_i(hkl) - \langle I(hkl)\rangle| / \sum_{hkl}\sum_i I_i(hkl)$, where $I(hkl)$ is the intensity of reflection hkl, $\sum_{hkl}$ is the sum over all reflections and $\sum_i$ is the sum over i measurements of reflection h.

NaCl. The protein was subjected to buffer-exchange to 10 m*M* potassium phosphate buffer pH 7.0 and loaded onto a Bio-Scale CHT10-I column (Bio-Rad) pre-equilibrated with the same buffer. The protein was bound to the column and eluted with a linear gradient from 10 to 450 m*M* potassium phosphate buffer pH 7.0. The protein was subjected to gel filtration on a HiLoad 16/60 Superdex 200 pg column (GE Healthcare Biosciences) pre-equilibrated with 20 m*M* Tris–HCl and 200 m*M* NaCl pH 8.0. The protein-containing fraction was collected and the purified *Ph*ThiK protein was concentrated using Vivaspin 10 kDa cutoff (Sartorius). The final preparation was dissolved in 20 m*M* Tris–HCl containing 200 m*M* NaCl and 1 m*M* DTT pH 8.0. The purity was greater than 95% as analyzed by SDS–PAGE. The protein concentration was determined by measuring the absorbance at 280 nm (Kuramitsu *et al.*, 1990). The yield of the purified protein was 1.9 mg per litre of culture.

2.2. Crystallization

Initial crystallization trials were attempted for the purified *Ph*ThiK protein (1.9 mg ml^{-1}) in 20 m*M* Tris–HCl pH 8.0 containing 200 m*M* NaCl and 1 m*M* DTT using commercially available kits from Hampton Research. Crystals were obtained employing the micro-batch-under-oil method with a 7:3 ratio of silicon and paraffin oils in Nunc HLA plates (Nalge Nunc International). Crystals suitable for X-ray diffraction studies grew in a few weeks at 293 K using 1 µl protein solution mixed with 1 µl of a solution containing 0.1 *M* CHESS buffer pH 9.3 and 0.88 *M* sodium citrate as the precipitant. After one month, crystals reached final dimensions of 0.20 × 0.20 × 0.35 mm. Prior to immersion in liquid nitrogen for storage and data collection, the crystals were transferred to mother liquor containing 25%(*v*/*v*) glycerol for cryoprotection.

2.3. X-ray data collection and analysis

Diffraction data were collected from a single crystal on the RIKEN Structural Genomics Beamline (BL26B1) at SPring-8 in Japan using a Rigaku R-AXIS VII image-plate detector (Rigaku MSC Co., Tokyo, Japan). The *Ph*ThiK crystal was briefly soaked in the mother liquor and was cooled in a nitrogen-gas stream at 100 K using the SPring-8 Precise Automatic Cryo-sample Exchanger (SPACE), which was controlled by *BSS* beamline-scheduling software (Ueno *et al.*, 2004, 2005). The wavelength of the incident X-ray beam was 1 Å and a total of 180 frames were recorded. Each diffraction frame was taken with

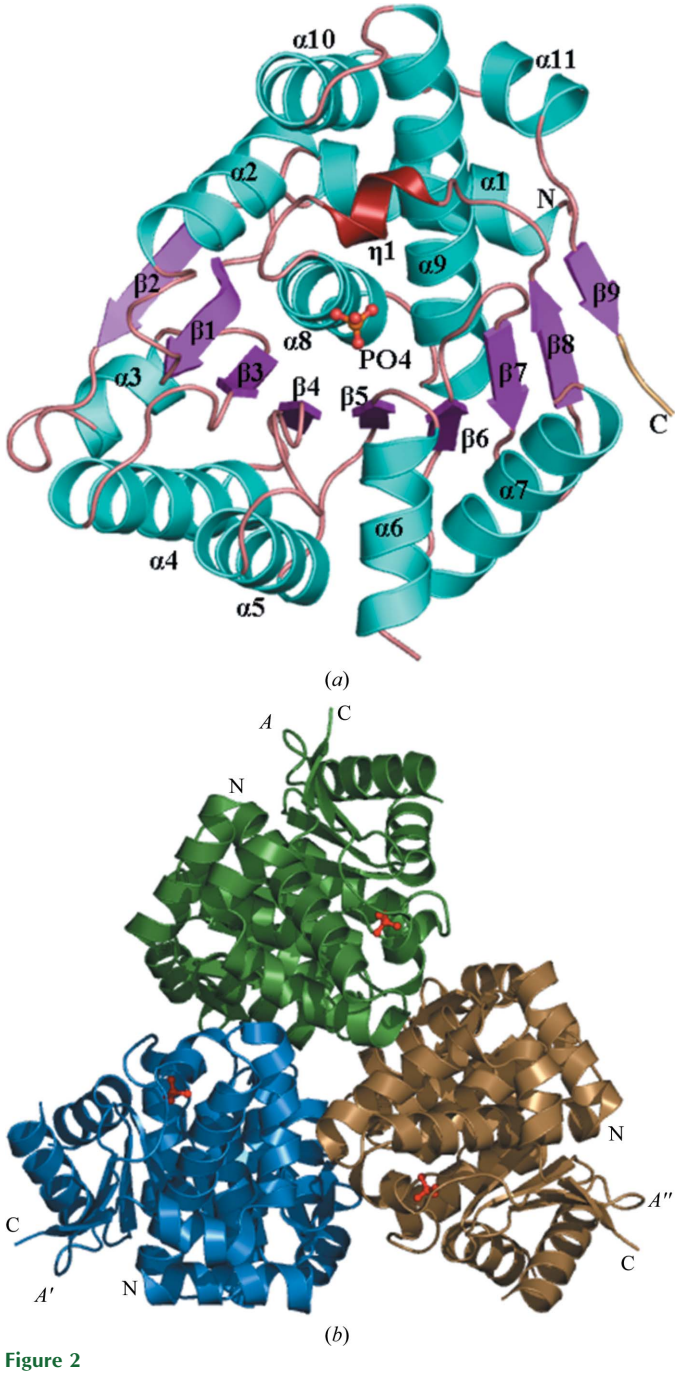

Figure 2
Ribbon diagram showing (*a*) the *Ph*ThiK subunit in the asymmetric unit and (*b*) the quaternary assembly of the trimeric *Ph*ThiK structure. The phosphate ion is shown in ball-and-stick representation. Symmetry-related molecules are indicated *A*′ and *A*″.

Table 2
Residues involved in hydrogen bonds between subunits in the *Ph*ThiK trimer.

	Subunits *A* and *B*			Subunits *B* and *C*			Subunits *A* and *C*		
	A	*B*	Distance (Å)	*B*	*C*	Distance (Å)	*A*	*C*	Distance (Å)
1	Val25 O	Asn28 ND2	2.90	Val25 O	Asn28 ND2	2.90	Asn28 ND2	Val25 O	2.90
2	Asp68 OD2	His45 NE2	2.86	Asp68 OD2	His45 NE2	2.86	Asn32 OD1	Thr191 N	2.66
3	Thr99 OG1	Glu49 OE1	2.78	Thr99 OG1	Glu49 OE1	2.78	Leu35 O	Arg189 NH1	2.99
4	Lys100 N	Glu52 OE1	2.79	Lys100 N	Glu52 OE1	2.79	His45 NE2	Asp68 OD2	2.86
5	Arg102 NE	Glu49 OE1	2.65	Arg102 NE	Glu49 OE1	2.65	Glu49 OE1	Thr99 OG1	2.79
6	Arg102 NH2	Glu49 OE2	2.93	Arg102 NH2	Glu49 OE2	2.93	Glu49 OE1	Arg102 NE	2.65
7	Arg189 NH1	Leu35 O	2.99	Arg189 NH1	Leu35 O	2.99	Glu49 OE2	Arg102 NH2	2.93
8	Thr191 N	Asn32 OD1	2.66	Thr191 N	Asn32 OD1	2.66	Glu52 OE1	Lys100 N	2.79
9	Gly236 N	Asp244 OD1	2.72	Gly236 N	Asp244 OD1	2.72	Asp244 OD1	Gly236 N	2.72
10	Ser237 N	Asp244 OD1	2.82	Ser237 N	Asp244 OD1	2.82	Asp244 OD1	Ser237 N	2.82
11	Ser237 OG	Asp244 OD2	2.53	Ser237 OG	Asp244 OD2	2.53	Asp244 OD2	Ser237 OG	2.53

an oscillation angle of 1° and an exposure time of 10 s. The crystal-to-detector distance was kept at 200 mm. The crystal diffracted to beyond 1.85 Å resolution and the completeness of the final data was 99.8%. The data were processed using *DENZO* and *SCALEPACK* from the *HKL*-2000 suite of programs (Otwinowski & Minor, 1997). Statistics related to data collection are given in Table 1.

2.4. Structure determination and refinement

The structure was determined by the molecular-replacement technique using the *AMoRe* software package (Navaza, 1994). One subunit of the *B. subtilis* ThiK (*Bs*ThiK) structure crystallized in a monoclinic space group (PDB code 1c3q; Campobasso *et al.*, 2000) was used as a search model. Calculation of rotation and translation functions using diffraction data between 10.0 and 4.0 Å resolution revealed a clear solution for a single subunit in the asymmetric unit with a correlation coefficient of 55% and an *R* factor of 46%. The initial model was subjected to rigid-body refinement. This was followed by positional refinement and simulated annealing using *CNS* (Brünger *et al.*, 1998). 5% of reflections were used for the calculation of $R_{\rm free}$ to monitor the progress of refinement. Both $2F_{\rm o} - F_{\rm c}$ and $F_{\rm o} - F_{\rm c}$ maps were calculated from the phases based on the roughly refined model at this stage. The atomic model was built using the programs *FRODO* (Jones, 1985) and *Coot* (Emsley & Cowtan, 2004) in an iterative manner. The composite OMIT map was calculated at different stages of refinement in order to remove model bias. The *R* factor fell to below 30% using *Coot* (Emsley & Cowtan, 2004) and solvent molecules were gradually added to the model based on electron densities above 0.9σ and 2.8σ in $2F_{\rm o} - F_{\rm c}$ and $F_{\rm o} - F_{\rm c}$ maps, respectively. Interestingly, we found a blob of positive electron density at the active site that could be interpreted as a phosphate ion and this was included in the model. At this stage, individual *B*-factor refinement was started and additional water molecules were included in the subsequent refinement cycle. The residues 132–143, which are part of a flexible loop, and the last residue (Leu265) of the C-terminal region could not be located in the electron-density map. The final *R* and $R_{\rm free}$ values were 16.4 and 18.4%, respectively, and the stereochemical quality of the structure was validated using *PROCHECK* (Laskowski *et al.*, 1993). Statistics of the structural refinement and validation of the model are provided in Table 1.

2.5. Molecular modelling

The refined model of *Ph*ThiK was used for modelling studies after removing water molecules and the phosphate ion. Since no structures are available for complexes with the reactants or the products released after catalysis, this prompted us to model ADP and phosphorylated hydroxyethylthiazole (THZ-P) complexed with the refined *Ph*ThiK model based on the structures of the complexes of *Bs*ThiK and *Ef*ThiK. The complex of the reactant ATP and the substrate hydroxyethylthiazole (THZ) with *Ph*ThiK was also modelled in order to compare it with the available structures of *Bs*ThiK complexes (Campobasso *et al.*, 2000). The ternary *Ph*ThiK–ADP–THZ-P complex was constructed by superimposing the C198S mutant of the *Bs*ThiK complex (PDB code 1esq; Campobasso *et al.*, 2000) for THZ-P and using the *Ef*ThiK complex for ADP (PDB code 3dzv; Joint Center for Structural Genomics, unpublished work). Subsequently, a 5 Å water shell was generated around the ADP and THZ-P of the complex using *Insight* II (Accelrys Inc, San Diego, California, USA). After generating H atoms, the modelled complex was subjected to 100 cycles of steepest-descent energy minimization followed by conjugate-gradient energy minimization. The CVFF force field was used with a distance-dependent dielectric constant of unity. The protein C^{α}-trace atoms were tethered harmonically with a force constant of 419 kJ $Å^{-2}$. The remaining atoms in the model were allowed to move freely during minimization. The model of the ternary complex of *Ph*ThiK with the reactant ATP and THZ was minimized in a similar manner to the model of the ternary complex of *Ph*ThiK with ADP and THZ-P.

3. Results and discussion

3.1. Quality of the *Ph*ThiK model

The crystal structure of 4-methyl-5-β-hydroxyethylthiazole kinase from *P. horikoshii* OT3 (*Ph*ThiK) was solved by the molecular-replacement method. The asymmetric unit contained a single subunit with a phosphate ion at the binding pocket as represented in Fig. 2(*a*). The *Ph*ThiK structure was refined to an *R* factor of 16.4% ($R_{\rm free}$ = 18.4%) at 1.85 Å resolution with standard deviations of bond lengths and bond angles of 0.005 Å and 1.3°, respectively. The final model of the enzyme consisted of 253 amino acids (residues 1–132 and 144–264), one phosphate ion and 208 water molecules. Residues 132–143, which are part of a flexible loop connecting helices α6 and α7, were disordered and the carboxy-terminal residue Leu265 was not visible in the electron-density maps. The quality of the refined protein model assessed using the program *PROCHECK* (Laskowski *et al.*, 1993) showed that none of the residues were in the disallowed region of the Ramachandran plot. The structural superposition was carried out using *ALIGN* (Cohen, 1997) and surface areas were calculated using *NACCESS* (http://www.bioinf.manchester.ac.uk/naccess/). Figures were prepared using the program *PyMOL* (DeLano, 2002).

3.2. Trimeric structure of *Ph*ThiK

The *Ph*ThiK monomer in the asymmetric unit and its threefold-related partner constitute a trimer resembling those of the *Bs*ThiK

(Campobasso *et al.*, 2000) and *Ef*ThiK structures. The trimeric assembly of *Ph*ThiK can be described as a symmetrically triangular-shaped arrangement with dimensions of 75 × 66 × 45 Å (Fig. 2*b*). In the trimeric crystal structure, intersubunit interfaces are formed with threefold symmetry-related partners by extensive hydrophobic interactions and hydrogen bonds including ion-pair interactions. The residues involved in hydrogen bonds between subunits are listed in Table 2. The hydrophobic interactions are formed by residues from helices (α2 and α10), η1 and various loops; these connect β1α2, β3α4, β4α5, η1α8 and α9α10 of molecule *A* with helices (α2, α3 and α10), β2 and residues forming part of loops (α1β1, β1α2, α2β2, β2α3) of the symmetry-equivalent molecule.

3.3. Structure of *Ph*ThiK monomer

The monomeric structure of *Ph*ThiK in the asymmetric unit belongs to the ribokinase superfamily. The topology of the *Ph*ThiK structure shows the typical ribokinase fold (Campobasso *et al.*, 2000; Sigrell *et al.*, 1998; Mathews *et al.*, 1998) of an α/β protein comprising of 11 α-helices, one 3_{10}-helix and a nine-stranded mixed β-sheet that has topology β2, β1, β3, β4, β5, β6, β7, β8, β9 (Fig. 2*a*). As observed in other available three-dimensional ThiK structures, the first six strands (β2, β1, β3, β4, β5 and β6) are parallel to each other, whereas strands β6, β7, β8 and β9 are antiparallel. Helices α3, α4, α5, α6 and α7 flank one side of the central β-sheet and the remaining seven helices including a 3_{10}-helix (η1) form a bundle on the opposite side. Helices α2, α9 and α10 form a bundle adjoining the β-sheet.

Inspection of the difference electron-density map during the final stage of refinement showed a positive density peak in the region of the expected nucleotide-binding site into which a phosphate ion could be unambiguously fitted. The average *B* factor of the phosphate ion was 45.4 Å^2. The phosphate ion occupies the position of the β-phosphate of ATP/ADP when the *Bs*ThiK and *Ef*ThiK complexes are superimposed. There is a direct hydrogen bond between one of the phosphate O atoms (O2) and Gly194 N. Moreover, water molecules form a cluster occupying both the nucleotide-binding and

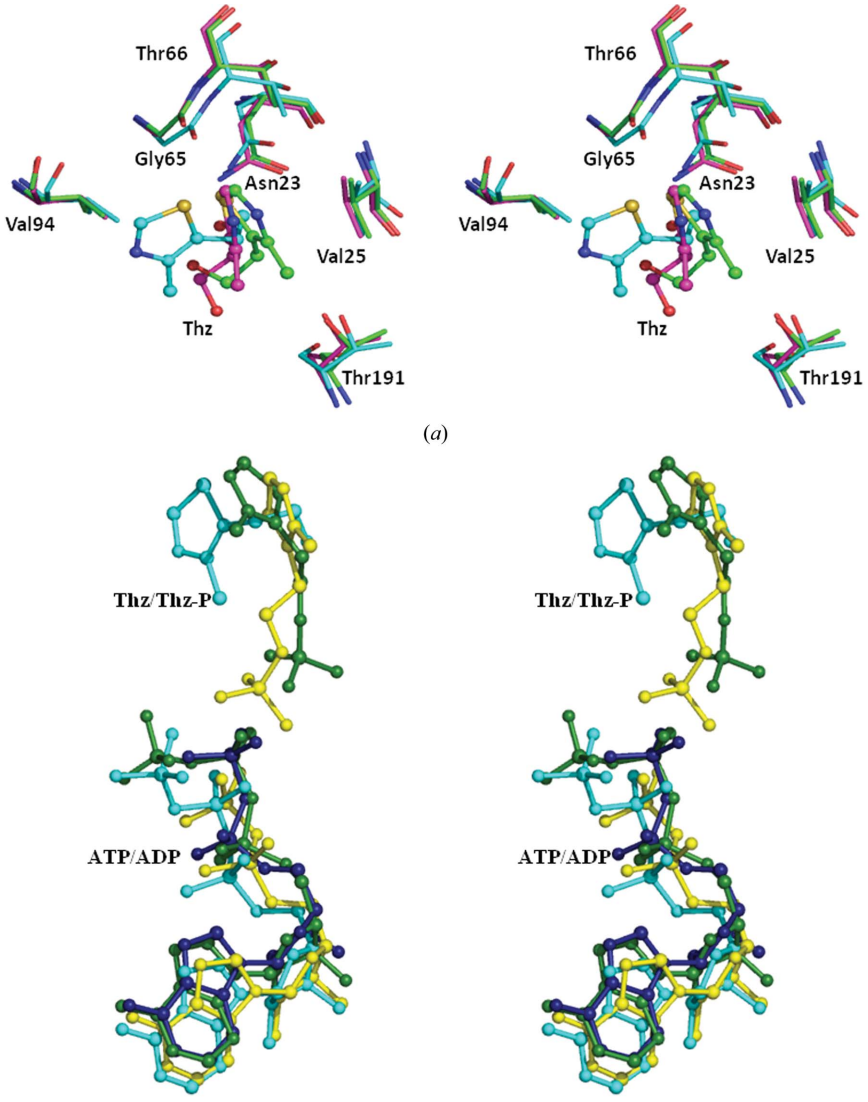

Figure 3
(*a*) Stereoview showing the overlay of residues involved in the binding site of thiazole in the energy-minimized model of *Ph*ThiK and the crystal structures of *Bs*ThiK complexes. The ligand atoms are shown in ball-and-stick representation and the *Ph*ThiK (cyan) residue numbering is indicated. The *R*3 and $P2_1$ forms of *Bs*ThiK are depicted in green and magenta, respectively. (*b*) The relative orientation of nucleotide and substrate with respect to protein in energy-minimized models of *Ph*ThiK (cyan and yellow), the mutant complex of *Bs*ThiK (green) and *Ef*ThiK (blue).

substrate-binding site cleft. The phosphate ion also interacts with the protein through water molecules. The residues involved in the water-mediated interactions are Lys118, Thr165, Leu187, Val190, Gly192 and Thr193. Also noteworthy is the water molecule (165) that occupies the position of the thiazole S atom that interacts with the backbone O atom of Gly65. Among the interacting residues, Gly65, Thr165, Leu187, Gly192 and Gly194 are identical in *Ph*ThiK, *Bs*ThiK and *Ef*ThiK.

3.4. Docking of ternary complexes of *Ph*ThiK

In the ribokinase-like kinases, the highly conserved Asp residue (replaced by Cys195 in *Ph*ThiK and Cys198 in *Bs*ThiK) is believed to serve as a catalytic base during the phosphorylation process. Since there are no structural models of the complexes with the reactants as well as with the products that are released upon the catalytic reaction of ThiK enzymes, we modelled the binding modes for the products ADP/THZ-P and reactants ATP/THZ with *Ph*ThiK as described in §2. The residues involved in the active site are indicated in Fig. 1. The active site is located at the interface between adjacent subunits. Each active site contains a thiazole-binding site and a nucleotide-binding site.

3.4.1. Thiazole binding site. The phosphorylated hydroxyethylthiazole (THZ-P) and ADP conformations from the energy-minimized model do not substantially deviate from the crystallographically observed models. In the energy-minimized model of the ATP/THZ complex the orientation of the thiazole moiety of the substrate THZ is different, as can be seen in Figs. 3(*a*) and 3(*b*), when compared with other complexes (Campobasso *et al.*, 2000). However, the interactions of THZ are nearly the same as those observed in other complexes. In the energy-minimized model, the THZ molecule interacts with the highly conserved residues Asn23, Gly65 and Val94. In the *Bs*ThiK complexes one face of the thiazole ring stacks against Val27 (Val25 in *Ph*ThiK), while the opposite face is more solvent-exposed. Interestingly, the thiazole ring in the *Ph*ThiK complex is moved towards Val94 and away from Val25. Interestingly, despite the difference in the relative orientation of the thiazole ring, the side chain of the catalytic Cys195 is also located at the bottom of the active site near to the hydroxyl group of the THZ in the energy-minimized model of *Ph*ThiK. The relative orientation of the residues involved in thiazole binding is nearly the same in both *Bs*ThiK and the *Ph*ThiK energy-minimized model (Fig. 3*a*).

The interactions between phosphorylated hydroxyethylthiazole and protein in the energy-minimized model of *Ph*ThiK are nearly the same as observed in the mutant complex of *Bs*ThiK, even though the THZ-P molecule points towards the β-phosphate of ADP. The phosphate O atoms of THZ-P are 3.2 and 3.5 Å from the β-phosphate of ADP. The thiazole S atom interacts with Gly65 O and the phosphate group of THZ-P is involved in hydrogen-bonding interactions with the backbone N atoms of Thr193 and Gly194 and with Cys195 SG. The side chain of Thr191 and the backbone atoms of Gly192 and Gly194 are only involved in van der Waals interactions.

3.4.2. Nucleotide binding site. In the *Bs*ThiK complex the ATP molecule stretches out along the C-terminal edge of the central β-sheet and is closest to strands β5, β6, β7 and β8. The adenine base is stacked between two loops. One of the loops connects β6 and β7 and the other loop is positioned before the 3_{10}-helix. There are no hydrogen bonds between the adenine base and the protein (Campobasso *et al.*, 2000). The relative orientations of the substrate and the nucleotide with respect to the protein in the energy-minimized models of *Ph*ThiK and the crystal structures of *Bs*ThiK and *Ef*ThiK are shown in Fig. 3(*b*). Interestingly, in the energy-minimized model of the *Ph*ThiK complex the adenine N atoms are involved in hydrogen-bonding interactions with the backbone O atoms of the highly conserved Gly166 and Ala167. The backbone O atom of Asn182 also makes interactions with the adenine N atom. A similar interaction could also be inferred from the *Ef*ThiK complex. However, in the *Ef*ThiK complex the former two residues make contacts with sugar O atoms and the latter is similar to that of the *Ph*ThiK model. The adenine moiety of ADP makes hydrogen bonds to the backbone O atoms of Gly166 and Ala167 located in a loop between β6 and β7 on one side and the backbone O atoms of Asn182 and His184 on the other. The sugar ring of ADP mainly interacts with Asn182 O and the side chain of Asp169. Leu187 and Leu218 are only involved in van der Waals interactions with the sugar ring. The guanidinium moiety of the conserved Arg121 in the C198S-mutant *Bs*ThiK–ATP–THZ-P complex provides an additional electrostatic stabilization of the β-phosphate. The same interaction is also observed in the energy-minimized model of the *Ph*ThiK complex. However, this interaction is made *via* a water-molecule bridge in the *Ef*ThiK complex. In the energy-minimized model of *Ph*ThiK–ATP–THZ the ATP interactions with the enzyme are nearly similar to those in the C198S mutant of the *Bs*ThiK complex.

3.5. Structural comparison

A detailed comparative study between *Ph*ThiK and the two available ThiK structures from *B. subtilis* [wild type, PDB code 1ekq;

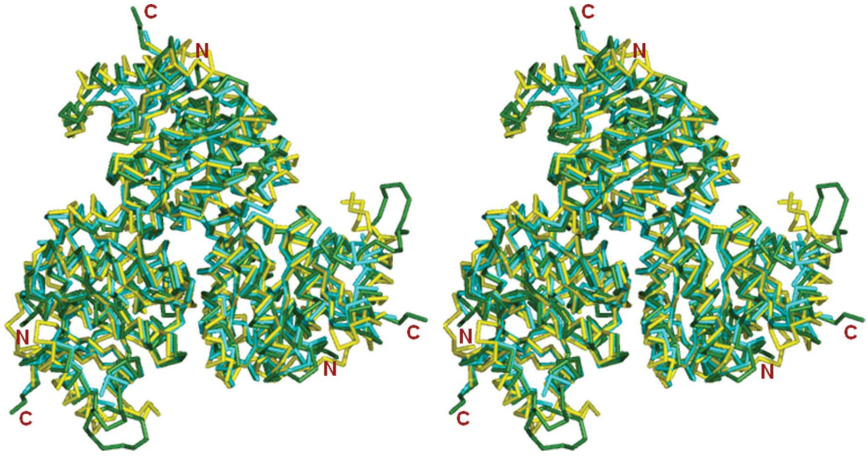

Figure 4
Stereo drawing of the structural superposition of the trimer of *Ph*ThiK (cyan) with trimers of *Bs*ThiK (green) and *Ef*ThiK (yellow).

wild-type complex with hydroxyethylthiazole (THZ) in *R*3 form, PDB code 1ekk; wild-type complex with THZ in $P2_1$ form, PDB code 1c3q; C198S mutant, PDB code 1esj; C198S mutant complex with phosphorylated THZ and ATP; PDB code 1esq] and *E. faecalis* V583 (wild-type complex with ADP; PDB code 3dzv) was carried out to explore the influence of the substrate and nucleotide binding on the tertiary and quaternary structure of ThiK.

3.5.1. Comparison of trimer. *Ph*ThiK has a sequence identity of 41% with *Bs*ThiK and of 25% with *Ef*ThiK, although the amino-acid sequences show considerable divergence outside of the binding-site and interfacial regions (Fig. 5). The overall structures from all three species closely resemble one another.

*Ph*ThiK exists as a monomer in the asymmetric unit and the trimer is formed with its symmetry partner, whereas the *R*3 form of *Bs*ThiK crystallized in two crystallographically independent subunits and each subunit further makes trimers with its symmetry equivalent. These two trimers are related by noncrystallographic translational symmetry. In the $P2_1$ form of *Bs*ThiK a single trimer exists in the asymmetric unit. All of the residues are only observed in the *R*3 and $P2_1$ forms of the wild type–THZ complexes. The residues in the loop that connects α6 and α7 are disordered in all remaining ThiK structures from all three species, including the wild-type and mutant *Bs*ThiK complexes. In the wild-type *Bs*ThiK structure this loop mainly interacts with some of the residues in α6 and also with the side chain (CB) of the conserved Asn123 (Asn120 in *Ph*ThiK and Asn121 in *Ef*ThiK). This hydrophobic interaction appears in both subunits. Interestingly, the side chain of this conserved Asn residue interacts with the γ-phosphate of the nucleotide in the mutant complex of *Bs*ThiK, whereas the β-phosphate is involved in this interaction in both *Ef*ThiK and the energy-minimized models of *Ph*ThiK. When the *Ph*ThiK trimer is superimposed on the trimers of different forms of wild-type as well as mutant *Bs*ThiK complexes, 735–749 pairs of C^{α} positions superpose with an r.m.s.d. ranging from 0.9 to 1.3 Å (Fig. 4).

In *Ef*ThiK, the two subunits are related by 2_1 screw symmetry in the asymmetric unit and each subunit further generates a trimer with its symmetry-related subunits. When the *Ph*ThiK trimer is superimposed on the trimers of the *Ef*ThiK complex, 687–705 pairs of C^{α} positions superpose with r.m.s.d. ranging from 1.3 to 1.4 Å (Fig. 4). Interestingly, a salt bridge is formed between the side chain of Arg49 of subunit *A* and Glu73 of subunit *B* in the asymmetric unit of *Ef*ThiK. The former positively charged residue is replaced by the negatively charged Glu48 in *Ph*ThiK and Glu50 in *Bs*ThiK, while the latter negatively charged residue is replaced by Arg72 in *Ph*ThiK and Val74 in *Bs*ThiK. Therefore, this ion-pair interaction is absent in both *Ph*ThiK and *Bs*ThiK. However, the corresponding structural equivalent of these residues is situated at the threefold interface in the *Ph*ThiK and *Bs*ThiK structures. It is worth mentioning that the residues involved in the twofold interface other than ion-pair interactions in *Ef*ThiK are not involved in the threefold interface in the ThiK structures from these three species.

The intersubunit interactions in the *Ph*ThiK structure are more extensive than those in the *Bs*ThiK complexes. The surface area buried on trimer formation in the former is larger by about 977–1104 $Å^2$ than in the latter. It is only about 225 $Å^2$ lower in the case of the *Ef*ThiK complex. The interfacial regions of the molecule are nearly the same in all three species and they are also reflected in the numbers of intersubunit hydrogen bonds, which are nearly the same in all three species, except for trimer I of the wild-type *Bs*ThiK structure. However, there are differences in the number of residues involved in the interfacial regions in the three species. There are 160 intersubunit nonbonded contacts in the structure of *Ph*ThiK as calculated using *PDB-sum* (http://www.ebi.ac.uk/pdbsum/), whereas there are 150 in the case of trimer I of *Ef*ThiK and 135 in trimer II. There are approximately 95 intersubunit nonbonded contacts in wild-type *Bs*ThiK and 82 contacts in the *R*3 form of the wild type THZ complex, whereas 106 nonbonded contacts are observed in the monoclinic form of the wild type THZ complex of *Bs*ThiK. Interestingly, the intersubunit nonbonded contacts in *Ph*ThiK and *Bs*ThiK appeared to be more nonpolar than in the *Ef*ThiK complex. This is because some of the charged residues in the interfacial regions in *Ef*ThiK are replaced by either hydrophobic or neutral charged residues in the *Ph*ThiK and *Bs*ThiK structures. In particular, Glu25, Glu29, Asp47, His67 and Asp245 are located at the interface in *Ef*ThiK. The corresponding equivalent residues in *Ph*ThiK (*Bs*ThiK) are Phe24 (Asn26), Asn28 (Asn30), Ala46 (Ala48), Thr66 (Thr68) and Ser237 (Ser243). Thus, the trimeric structures of both the *Ph*ThiK and *Ef*ThiK complexes can be expected to be somewhat stabler than those of the *Bs*ThiK complexes.

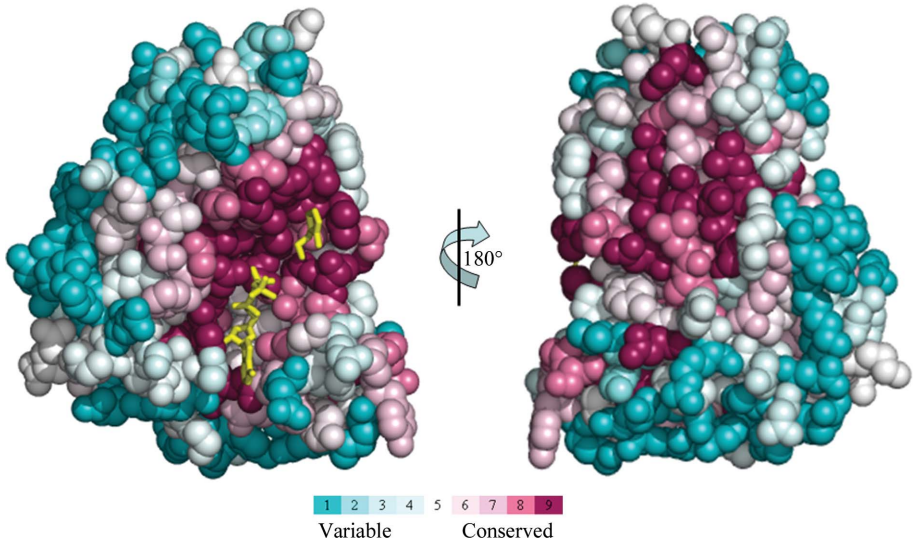

Figure 5
The evolutionary conservation score of the amino-acid positions in the 131 ThiK sequences calculated by the *CONSURF* server and mapped onto the structure of the *Ph*ThiK monomer. The two pictures are related by a rotation of 180° about the vertical axis. The right face of the picture on the left and the left face of that on the right approximately correspond to the intersubunit interface. The nucleotide and substrate are also shown as yellow stick models.

3.5.2. Comparison of monomers. When the *Ph*ThiK molecule was superimposed on the subunits of different forms of wild-type as well as mutant *Bs*ThiK complexes, 246–249 pairs of C^{α} positions superposed with r.m.s.d.s ranging from 0.9 to 1.0 Å. 238–244 pairs of C^{α} positions superposed with r.m.s.d.s ranging from 1.3 to 1.4 Å with substantial deviation in the N-terminal residues (some of which form the α1 helix) when *Ef*ThiK molecules were used for calculation. Thus, the tertiary and quaternary structures of ThiK are substantially unaffected by substrate and nucleotide binding.

3.6. Sequence analysis of ThiK

4-Methyl-5-β-hydroxyethylthiazole kinase sequences were extracted from the SWISS-PROT/TREMBL database with the *PSI-BLAST* algorithm using an *E*-value cutoff of 0.0001. The *Ef*ThiK sequence could not be detected when a *PSI-BLAST E*-value cutoff of 0.001 was used. A data set containing 131 unique sequences with less than 90% identity was constructed. The length of the sequences varied from 229 to 273 residues and the pairwise sequence identity varied from 25% to 82%. Multiple sequence alignment of these sequences was carried out using *ClustalW* (Thompson *et al.*, 1994). The ThiK sequences were spread over three groups: 115 sequences from bacteria, 14 sequences from archaea and two sequences from yeast. The eukaryotic yeast sequences contained two domains (thiamine-phosphate pyrophosphorylase and hydroxyethylthiazole kinase). The conservation scores for each residue position in the 131 sequences were calculated using the program *CONSURF* v.3.0 (Landau *et al.*, 2005) and were then mapped onto the three-dimensional structure of *Ph*ThiK (Fig. 5). The most highly conserved residues, indicated in maroon, are clustered around the substrate-binding and nucleotide-binding regions.

As indicated in Fig. 1, 41 residues fall into the most conserved regions based on an analysis of 131 unique ThiK sequences from various sources as calculated using *CONSURF* v.3.0 (Landau *et al.*, 2005). The residues involved in the nucleotide-binding and magnesium ion-binding sites fall into the most conserved regions. The residues involved in substrate binding, except for Leu187 in *Ph*ThiK, are also within the 41 most conserved residues. About 44 residues are involved in the intersubunit interfacial regions. Of these, 20 residues are highly conserved and 13 of them are conserved. The remaining 11 residues are variable. This indicates that 75% of the interfacial residues in the trimer are conserved. His45 and Asp68, which belong to a less conserved region, are involved in an intersubunit salt bridge. The residues involved in ATP/ADP binding and substrate binding in *Bs*ThiK and *Ef*ThiK are conserved. In ribokinase-like kinases (*e.g.* ribokinases, adenosine kinases and pyridoxal kinases), the highly conserved Asp residue (replaced by Cys195 in *Ph*ThiK) is believed to serve as a catalytic base during the phosphorylation process. It worth mentioning that only six sequences from Gram-positive bacteria, including *Ef*ThiK, have an Asp at this position; the other sequences contain Cys. This suggests that the majority of ThiKs utilize the Cys residue as an alternative catalytic base for the phosphorylation reaction. However, the specific activity of a mutant enzyme in which the Cys is replaced by Asp is ninefold higher than the native *Bs*ThiK enzyme (Campobasso *et al.*, 2000).

4. Conclusions

The crystal structure of *Ph*ThiK from *P. horikoshii* OT3 was determined at 1.85 Å resolution. The *Ph*ThiK structure reported here is the first of an archaeal ThiK enzyme. The phosphate ion occupies the position of the β-phosphate of the nucleotide as observed in *Bs*ThiK and *Ef*ThiK complexes. Sequence analysis of 131 ThiK sequences from various sources revealed that 41 residues fall into the most conserved regions. The active-site residues are highly conserved, showing that they may have the same catalytic properties as in *Bs*ThiK. In the crystal, ThiK molecules from three different sources form a trimer with crystallographic or noncrystallographic threefold symmetry, irrespective of whether they are of the unbound form and/or of the bound nucleotide/substrate complex.

JJ thanks beamlines BL12B2 and BL26B1 of SPring-8 for excellent facilities and assistance and also thanks the Bioinformatics Centre, Pondicherry University, Pondicherry, India. This work was supported by the RIKEN Structural Genomics/Proteomics Initiative (RSGI), the National Project on Protein Structural and Functional Analyses, Ministry of Education, Culture, Sports, Science and Technology of Japan.

References

Andersson, C. E. & Mowbray, S. L. (2002). *J. Mol. Biol.* **315**, 409–419.
Begley, T. P., Downs, D. M., Ealick, S. E., McLafferty, F. W., Van Loon, A. P. G. M., Taylor, S., Campobasso, N., Chiu, H.-J., Kinsland, C., Reddick, J. J. & Xi, J. (1999). *Arch. Microbiol.* **171**, 293–300.
Bellion, E., Kirkley, D. & Faust, J. (1976). *Biochim. Biophys. Acta*, **437**, 229–237.
Brünger, A. T., Adams, P. D., Clore, G. M., DeLano, W. L., Gros, P., Grosse-Kunstleve, R. W., Jiang, J.-S., Kuszewski, J., Nilges, M., Pannu, N. S., Read, R. J., Rice, L. M., Simonson, T. & Warren, G. L. (1998). *Acta Cryst.* D**54**, 905–921.
Campobasso, N., Mathews, I. I., Begley, T. P. & Ealick, S. E. (2000). *Biochemistry*, **39**, 7868–7877.
Cohen, G. E. (1997). *J. Appl. Cryst.* **30**, 1160–1161.
David, S., Estramareix, B., Fischer, J.-C. & Therisod, M. (1982). *J. Chem. Soc. Perkin Trans.* **1**, 2131–2137.
DeLano, W. L. (2002). *The PyMol Molecular Graphics System.* DeLano Scientific LLC, Palo Alto, California, USA.
Emsley, P. & Cowtan, K. (2004). *Acta Cryst.* D**60**, 2126–2132.
Estramareix, B. & Therisod, M. (1972). *Biochim. Biophys. Acta*, **273**, 275–282.
Gouet, P., Courcelle, E., Stuart, D. I. & Métoz, F. (1999). *Bioinformatics*, **15**, 305–308.
Himmeldirk, K., Kennedy, I. A., Hill, R. E., Sayer, B. G. & Spenser, I. D. (1996). *Chem. Commun.*, pp. 1187–1188.
Holm, L. & Sander, C. (1993). *J. Mol. Biol.* **233**, 123–138.
Jones, T. A. (1985). *Methods Enzymol.* **115**, 157–171.
Jurgenson, C. T., Begley, T. P. & Ealick, S. E. (2009). *Annu. Rev. Biochem.* **78**, 569–603.
Kawasaki, Y. (1993). *J. Bacteriol.* **175**, 5153–5158.
Kuramitsu, S., Hiromi, K., Hayashi, H., Morino, Y. & Kagamiyama, H. (1990). *Biochemistry*, **29**, 5469–5476.
Landau, M., Mayrose, I., Rosenberg, Y., Glaser, F., Martz, E., Pupko, T. & Ben-Tal, N. (2005). *Nucleic Acids Res.* **33**, W299–W302.
Laskowski, R. A., MacArthur, M. W., Moss, D. S. & Thornton, J. M. (1993). *J. Appl. Cryst.* **26**, 283–291.
Mathews, I. I., Erion, M. D. & Ealick, S. E. (1998). *Biochemistry*, **37**, 15607–15620.
McCulloch, K. M., Kinsland, C., Begley, T. P. & Ealick, S. E. (2008). *Biochemistry*, **47**, 3810–3821.
Navaza, J. (1994). *Acta Cryst.* A**50**, 157–163.
Newman, J. A., Das, S. K., Sedelnikova, S. E. & Rice, D. W. (2006). *J. Mol. Biol.* **363**, 520–530.
Nosaka, K., Nishimura, H., Kawasaki, Y., Tsujihara, T. & Iwashima, A. (1994). *J. Biol. Chem.* **269**, 30510–30516.
Otwinowski, Z. & Minor, W. (1997). *Methods Enzymol.* **276**, 307–326.
Petersen, L. & Downs, D. M. (1997). *J. Bacteriol.* **179**, 4894–4900.
Sigrell, J. A., Cameron, A. D., Jones, T. A. & Mowbray, S. L. (1998). *Structure*, **6**, 183–193.
Tazuya, K., Morisaki, M., Yamada, K., Kumaoka, H. & Saiki, K. (1987). *Biochem. Int.* **14**, 153–160.
Tazuya, K., Yamada, K., Nakamura, K. & Kumaoka, H. (1987). *Biochim. Biophys. Acta*, **924**, 210–215.

Thompson, J. D., Higgins, D. G. & Gibson, T. J. (1994). *Nucleic Acids Res.* **22**, 4673–4680.
Ueno, G., Hirose, R., Ida, K., Kumasaka, T. & Yamamoto, M. (2004). *J. Appl. Cryst.* **37**, 867–873.
Ueno, G., Kanda, H., Kumasaka, T. & Yamamoto, M. (2005). *J. Synchrotron Rad.* **12**, 380–384.
Zhang, Y., Taylor, S. V., Chiu, H.-J. & Begley, T. P. (1997). *J. Bacteriol.* **179**, 3030–3035.